LA-7454

C.3

Interaction of Explosive-Driven Air Shocks with Water and Plexiglas

University of California

LOS ALAMOS SCIENTIFIC LABORATORY
Post Office Box 1663 Los Alamos, New Mexico 87545

An Affirmative Action/Equal Opportunity Employer

UNITED STATES
DEPARTMENT OF ENERGY
CONTRACT W-7405-ENG. 36

LA-7454

UC-34
Issued: October 1978

Interaction of Explosive-Driven Air Shocks with Water and Plexiglas

Milton Dean Slaughter
B. W. Olinger
James D. Kershner
Charles L. Mader
Allen L. Bowman

INTERACTION OF EXPLOSIVE-DRIVEN AIR SHOCKS WITH WATER AND PLEXIGLAS

by

Milton Dean Slaughter, B. W. Olinger, James D. Kershner, Charles L. Mader, and Allen L. Bowman

ABSTRACT

The interaction of explosive-driven air shocks with water and Plexiglas has been investigated numerically. A 453.6-g cylinder of Pentolite was detonated 15.24 cm above a water surface and the subsequent pressure vs time profiles were calculated out to a test-scale depth of 0.6 m and test-scale range of 0.3 m using the *two-dimensional* Eulerian (2DE) hydrodynamic code. Mesh sizes of 0.5 and 0.25 cm were used. Calculated results agreed well with experiment—and improved as the mesh size was decreased. The air shock and Plexiglas problem was considered in both slab and spherical geometry. PBX 9404 was detonated at various distances from the Plexiglas and the pressure induced in the Plexiglas was calculated numerically as a function of time and distance using the SIN one-dimensional reactive-flow hydrodynamic Lagrangian code, as well as the 2DE code. Calculation and experiment agreed well.

I. INTRODUCTION

The results of numerical and experimental investigations of the interaction of explosive-driven air shocks with water and Plexiglas[1] are reported.

For the detonation, air, and water shock problem, a half-size model of a physical configuration was used for computation, with the expectation (backed by experiment) that any results, when multiplied by the appropriate dimensional scaling factor, would be valid for the physical situation. With this in mind, most of our results are presented in terms of "test-scale" quantities, already multiplied by the appropriate dimensional scaling factor. The studies were conducted in cylindrical geometry.

The numerical and experimental studies of the interaction of explosive-driven air shocks with Plexiglas (HE, air, and Plexiglas) were conducted in slab (plane) and spherical geometries. A slab or sphere of PBX 9404 was detonated in air at various distances from the Plexiglas. The pressure induced in the Plexiglas was then determined numerically and experimentally as a function of time. Section II details the detonation, air, and water shock problem and compares numerical and experimental results. Section III compares the results of the numerical and experimental studies of the HE, air, and Plexiglas system in slab geometry. Section IV compares the numerical and experimental results of an HE, air, and Plexiglas system in spherical geometry. Finally, Sec. V gives our conclusions about the efficacy and accuracy of our codes and equations of state.

II. DETONATION, AIR, AND WATER SHOCK

The detonation, air, and water shock problem was formulated in an effort to calculate the pressure induced in water by detonation of a 3.63-kg cylinder of Pentolite in air 30.48 cm above the water surface. Numerical computations actually were done with a half-scale model of the physical situation. Thus, a 453.6-g cylinder of Pentolite (with its major axis of symmetry perpendicular to the water surface) was center-detonated 15.24 cm (as measured from the geometric center of the cylinder) above the water surface and the interaction of the resulting air shock with the water was determined numerically out to a *test-scale* range of 0.3 m and a *test-scale* depth of 0.6 m when the 0.25-cm mesh was used and out to a *test-scale* depth of 0.6 m when the 0.5-cm mesh was used. The geometries are shown in Figs. 1 and 2 at the end of the report. Note that for the 0.5-cm mesh the 453.6-g cylinder of Pentolite was 2.5 cm in radius and 14.0 cm long, with its bottom 8.0 cm above the water surface; whereas for the 0.25-cm mesh it was 2.25 cm in radius and 17 cm long, with its bottom 6.5 cm above the water surface. Once the pressure induced in the water was known as a function of time (as well as range and depth), a number of interesting physical quantities were computed, such as shock factor, impulse flux, energy flux, peak overpressure, and effective duration.

The detonation, air, and water shock problem was first investigated in detail with a 0.5-cm mesh using the two-dimensional Eulerian (2DE) hydrodynamic code[2] running on the CDC-7600 computer.* The following calculational parameters were used.

Mesh size—0.5 cm
Mesh—150 x 100, or 15 000 cells
Miniumum pressure for mass movement—30 bars
Water viscosity—1.0×10^{-4}
Time step—0.10 μs for the first 100 cycles, 0.25 thereafter
Calculational time—8 s per cycle

*A major feature of the 2DE code is its ability to treat "true" mixed cells by use of the equation of state itself. This distinguishes our code from most others.

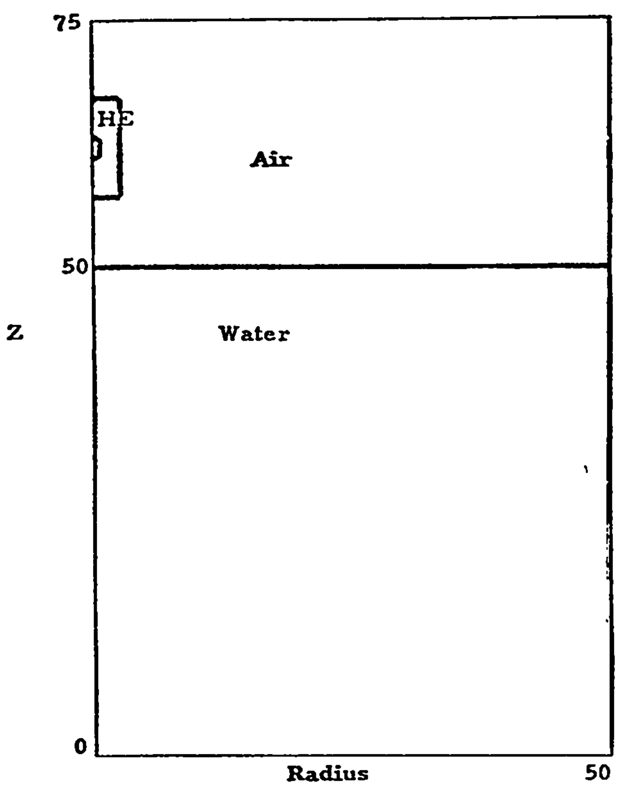

Fig. 1.
Initial geometry (0.5-cm mesh).

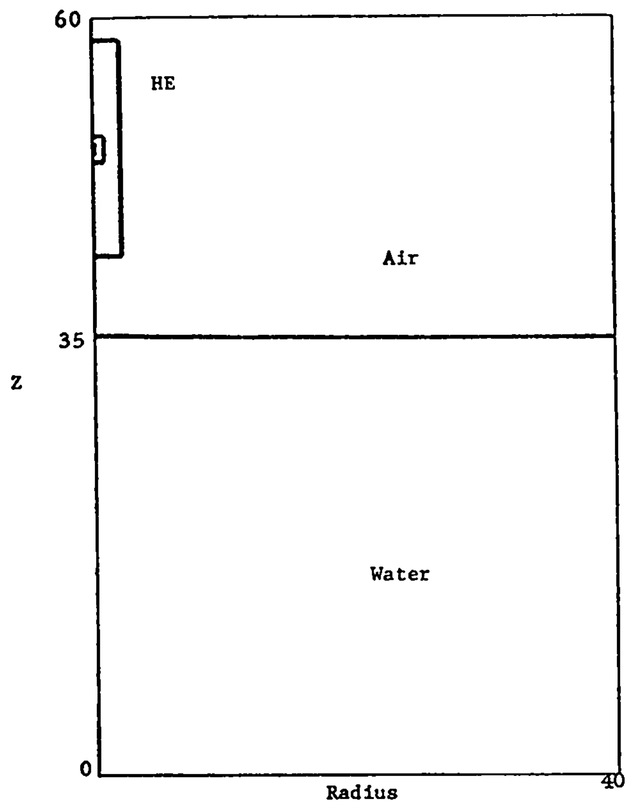

Fig. 2.
Initial geometry (0.25-cm mesh).

Figures 3 and 4 show the calculated and experimental pressure profiles as a function of time at test-scale depths of 0.3 and 0.6 m, respectively. In both cases agreement is poor, although the pressure profiles at the 0.6-m depth are better. Certainly a mesh smaller than 0.5 cm is necessary to "sharpen" the calculated peaks. Therefore, we turn to the 0.25-cm mesh.

The detonation, air, and water shock problem with the 0.25-cm mesh was solved on the CRAY computer, again using the 2DE hydrodynamic code and the following calculational parameters.

Mesh size—0.25 cm

Mesh—160 x 240, or 38 400 cells

Minimum pressure for mass movement—30 bars

Water viscosity—1×10^{-4}

Time step—0.05 μs for the first 200 cycles, 0.125 thereafter

Calculational time—≅ 6 s per cycle (equivalent to 20 s on 7600)

Table I (at the end of the text) gives the test-scale shock factor (Q_{FSF}) as a function of test-scale depth (D) when the range is zero. Q_{FSF} is given by

$$Q_{FSF} = \sqrt{\lambda}\, Q_{ESF} \quad ,$$

where $\lambda \equiv$ scale factor = 2. Q_{ESF} is the equivalent shock factor, defined by

$$Q_{ESF} = 1/2(0.0008480625456\ P^{0.491}\sqrt{I}$$

$$+\ 0.001681556947\ P^{-0.0177}\ \sqrt{E}) \quad ,$$

where

P = pressure in megapascals,

I = impulse flux in pascals per second

E = energy flux in pascals per meter

Mathematically, we have

$$I = \int P\, dt \ ,$$

$$E = (\int P^2\, dt)\, (\rho c)^{-1} \ ,$$

where the integrals are taken over the positive duration of P and $\rho c \equiv$ acoustic impedance ≅ 1.450 (kg/m³)(m/s). Note that an excellent power law fit can be made for Q_{FSF} vs D. Assuming that

$$Q_{FSF} = aD^b \quad (R = O) \quad ,$$

we find that a = 0.1306 and b = −1.0185 if D is in meters. The regression coefficient is 0.998. This simple fit predicts that Q_{FSF} ≅ 0.107 (experimental

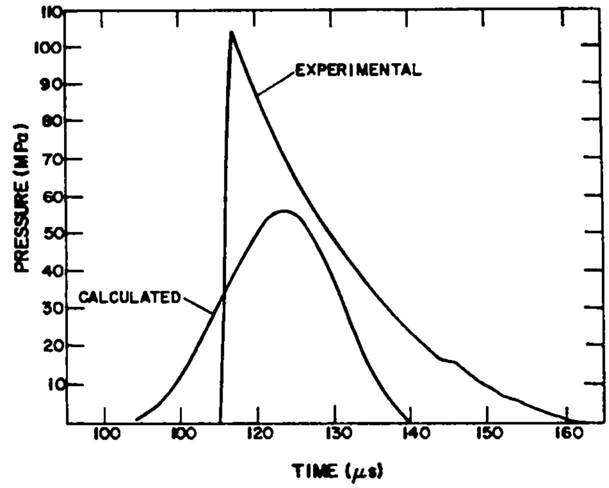

Fig. 3.
Calculated and experimental pressure vs time at a test-scale range of 0 m and test-scale depth of 0.3 m (0.5-cm mesh).

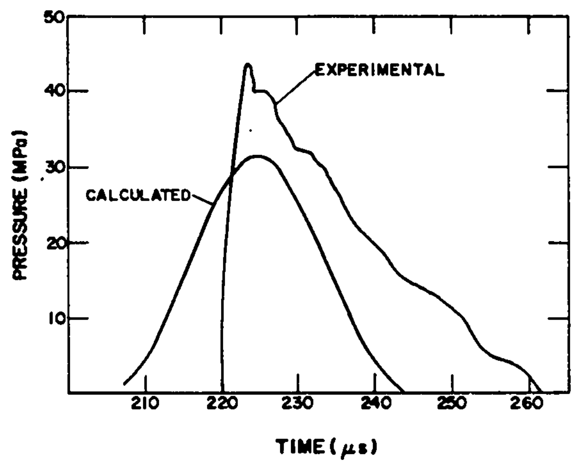

Fig. 4.
Calculated and experimental pressure vs time at a test-scale range of 0 m and test-scale depth of 0.6 m (0.5-cm mesh).

TABLE I

TEST-SCALE SHOCK FACTORS[a]
(Range = 0 m)

Depth (m)	Shock Factor
0.1	1.322
0.2	0.692
0.3	0.460
	(0.524)[b]
0.4	0.333
0.5	0.263
0.6	0.214
	(0.252)[b]

[a]Derived from calculations with 453.6-g Pentolite cylinders at 15.24-cm height of burst (h.o.b.) and experiments with 3.63-kg Pentolite cylinders at 30.48-cm h.o.b.
[b]Experimental value.

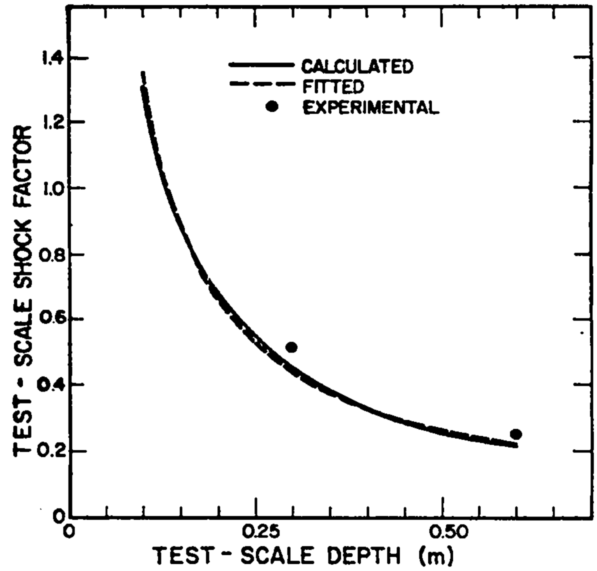

Fig. 5.
Test-scale shock factor vs test-scale depth.

value is 0.125)[1] when D = 121.92 cm, ≅ 0.071 when D = 182.88 cm, and ≅ 0.053 (experimental value is 0.054)[1] when D = 243.84 cm. These values compare well with experimental data[1] on R = O.

Figure 5 illustrates Q_{FSF} vs D for the experimental data, calculated curve, and fitted power law curve.

Figure 6 shows the calculated and fitted peak pressure (P_+) vs test-scale depth. Again, a power law fit suffices very well. It is given by

$$P_+ = a_1 D^{b_1} \quad (R = O) \ ,$$

where a_1 = 27.935 MPa, b_1 = −1.1263, D is in meters, and the regression coefficient is 0.9996.

Figure 7 shows the calculated and fitted equivalent scale impulse flux (I) vs test-scale depth. The power law fit is adequate and is represented by

$$I = a_2 D^{b_2} \quad (R = O) \ ,$$

where a_2 = 310.465 Pa-s, b_2 = −1.0407, D is in meters, and the regression coefficient is 0.9939.

Figures 8-20 are the calculated and experimental pressure-time profiles. Note from Figs. 12 and 17 that the calculated and experimental pressure time profiles agree well, particularly with respect to pulse width (effective duration) and peak pressure, the two most important physical quantities of interest.

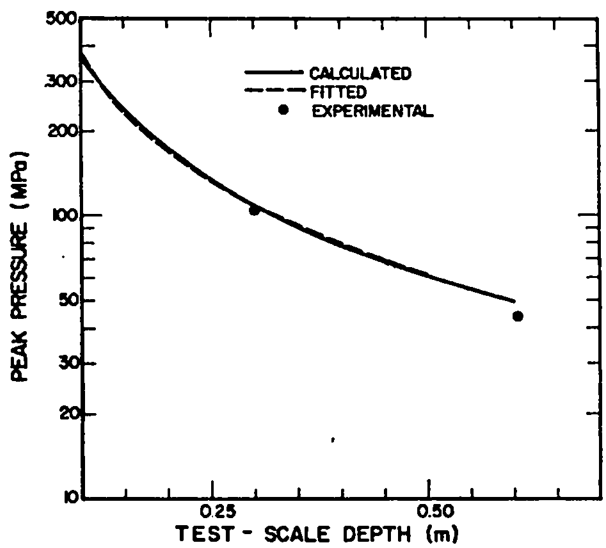

Fig. 6.
Peak pressure vs test-scale depth.

Overall pulse shape also agrees well. Presumably, use of a finer mesh would "sharpen" the profiles—especially at the shock front—and thereby allow for even better calculation. Figure 21 is the isobar plot for various times of run.

Finally, we give complete results of our calculation. Note that the reported impulse and energy

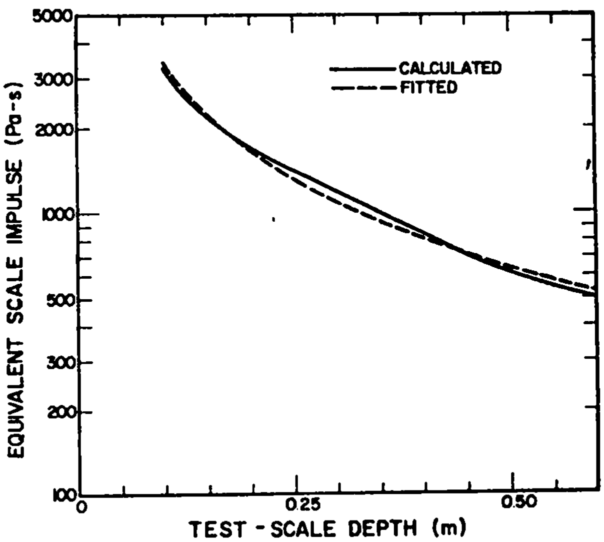

Fig. 7.
Equivalent scale impulse flux vs test-scale depth.

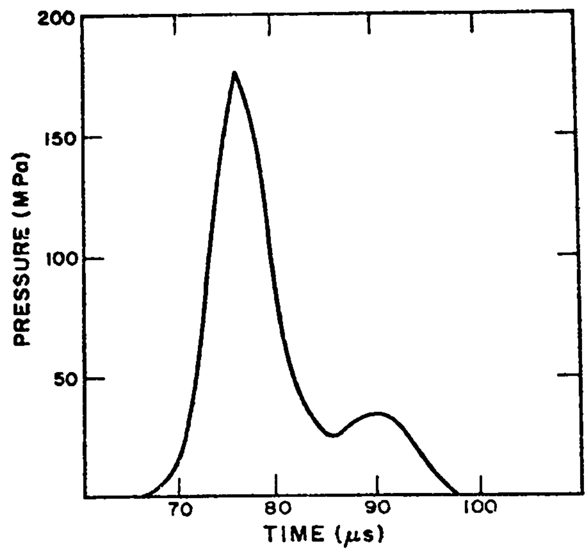

Fig. 9.
Calculated pressure vs equivalent scale time at a test-scale depth of 0.2 m and test-scale range of 0 m.

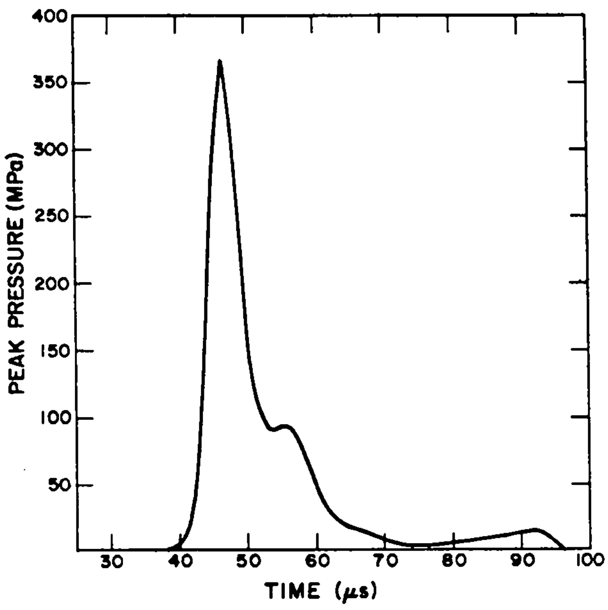

Fig. 8.
Calculated pressure vs equivalent scale time at a test-scale depth of 0.1 m and test-scale range of 0 m.

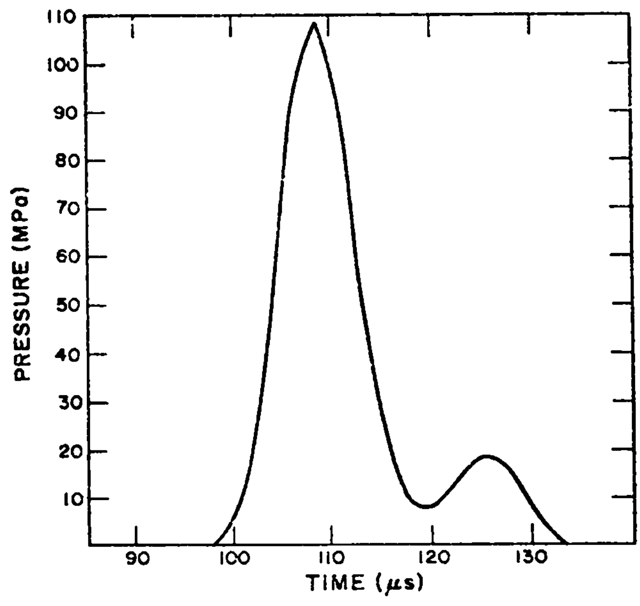

Fig. 10.
Calculated pressure vs equivalent scale time at a test-scale depth of 0.3 m and test-scale range of 0 m.

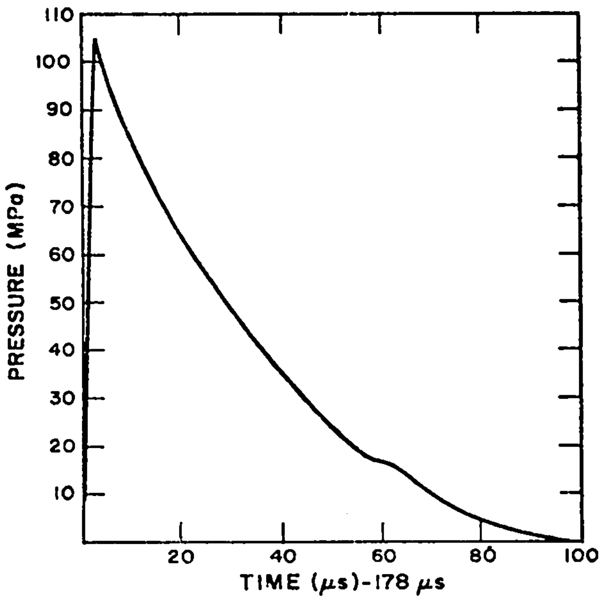

Fig. 11.
Experimental pressure from 3.63-kg Pentolite cylinders at 0.3048 m height of burst (h.o.b.) vs experimental time at a test-scale depth of 0.3 m and test-scale range of 0 m.

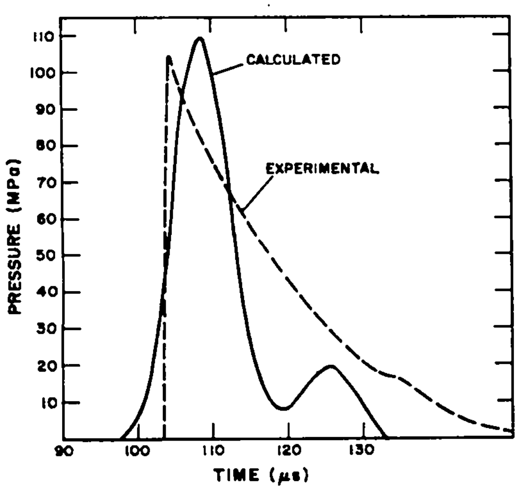

Fig. 12.
The pressure profiles of Figs. 10 and 11. Note that the time of Fig. 11 has been scaled down to the equivalent time of Fig. 10.

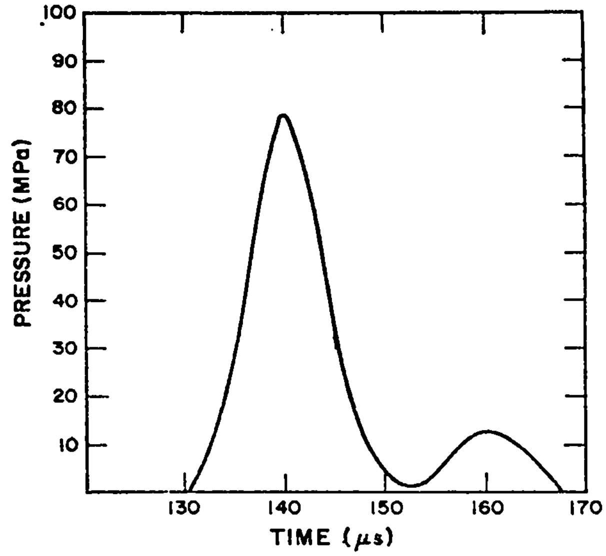

Fig. 13.
Calculated pressure vs equivalent scale time at a test-scale depth of 0.4 m and test-scale range of 0 m.

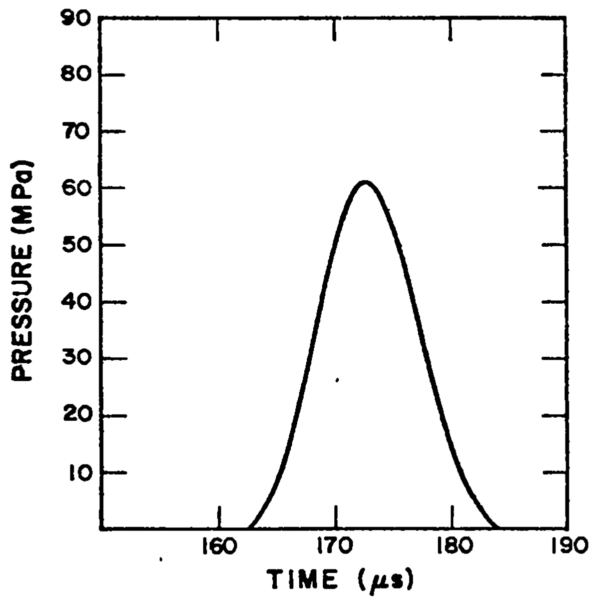

Fig. 14.
Calculated pressure vs equivalent scale time at a test-scale depth of 0.5 m and test-scale range of 0 m.

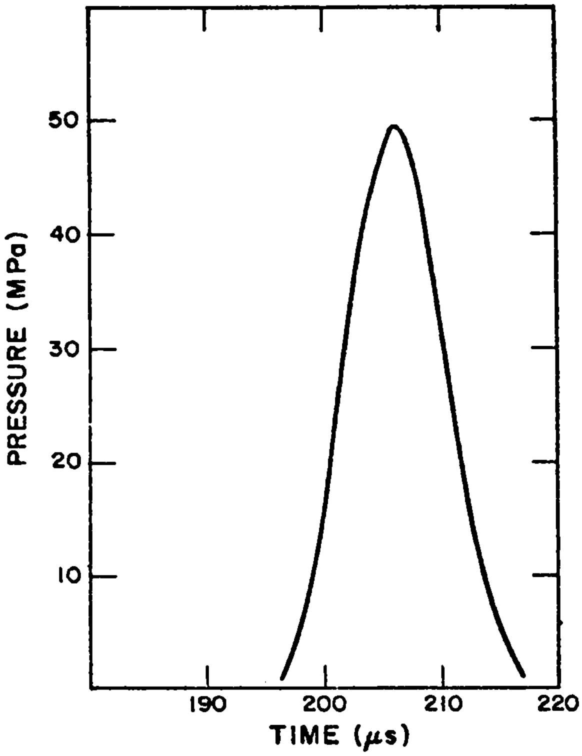

Fig. 15.
Calculated pressure vs equivalent scale time at a test-scale depth of 0.6 m and test-scale range of 0 m.

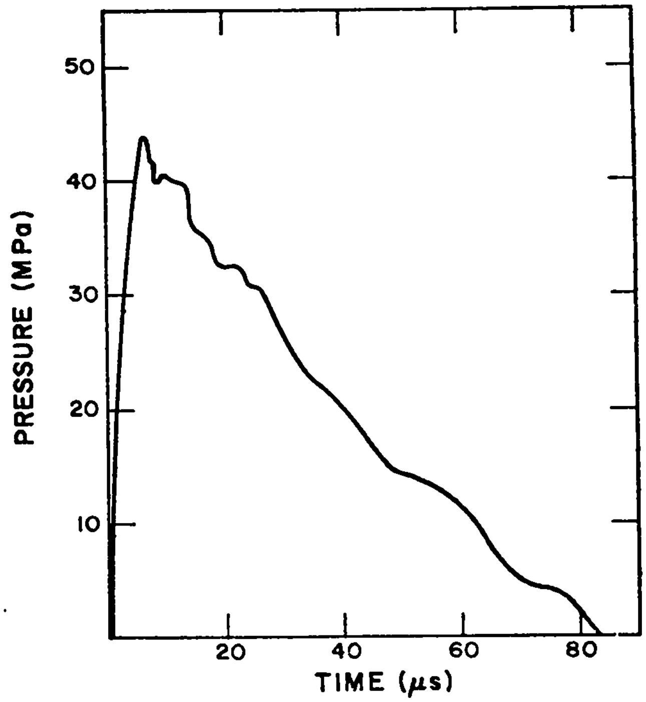

Fig. 16.
Experimental pressure from 3.63-kg Pentolite cylinders at 30.48 cm h.o.b. vs experimental time at a test-scale depth of 0.6 m and test-scale range of 0 m.

fluxes are equivalent scale quantities. They are as follows.

0.1 m Deep on Axis
Impulse flux = 3245.1013 Pa-s
Acoustic impedance = 1.450 (kg/m³)(m/s)
Energy flux = 429390.9769 m-Pa
Effective duration = 56.38 μs
Peak Pressure = 367.0300 MPa at 46.78 μs
Equivalent shock factor = 0.9351
Scale factor = 2.0000
Test-scale shock factor = 1.3224

0.2 m Deep on Axis
Impulse flux = 1698.4421 Pa-s
Acoustic impedance = 1.450 (kg/m³)(m/s)
Energy flux = 122393.4862 m-Pa
Effective duration = 30.38 μs
Peak pressure = 175.6400 MPa at 76.53 μs
Equivalent shock factor = 0.4895
Scale factor = 2.000
Test-scale shock factor = 0.6923

0.3 m Deep on Axis
Impulse flux = 1170.8748 Pa-s
Acoustic impedance = 1.450 (kg/m³)(m/s)
Energy flux = 54296.7192 m-Pa
Effective duration = 34.62 μs
Peak pressure = 109.0800 MPa at 108.15 μs
Equivalent shock factor = 0.3256
Scale factor = 2.0000
Test-scale shock factor = 0.4604

0.4 m Deep on Axis
Impulse flux = 839.7426 Pa-s
Acoustic impedance = 1.450 (kg/m³)(m/s)
Energy flux = 28128.2770 m-Pa
Effective duration = 36.76 μs

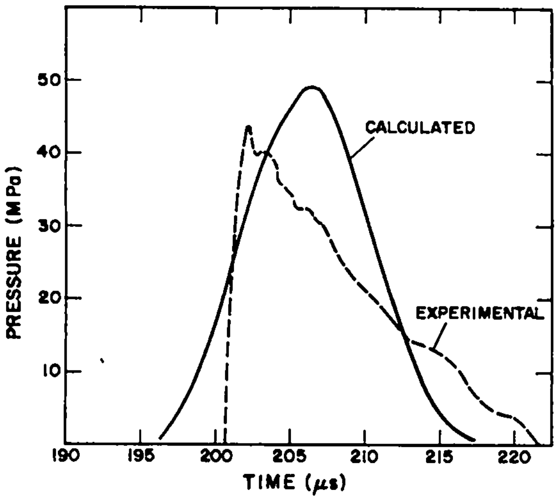

Fig. 17.
The pressure profiles of Figs. 15 and 16. Note that the time of Fig. 16 has been scaled down to the equivalent time of Fig. 15.

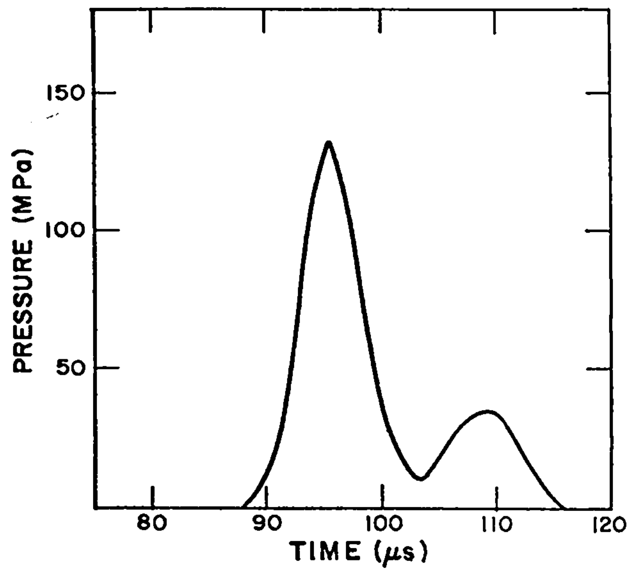

Fig. 19.
Calculated pressure vs equivalent scale time at a test-scale depth of 0.2 m and test-scale range of 0.2 m.

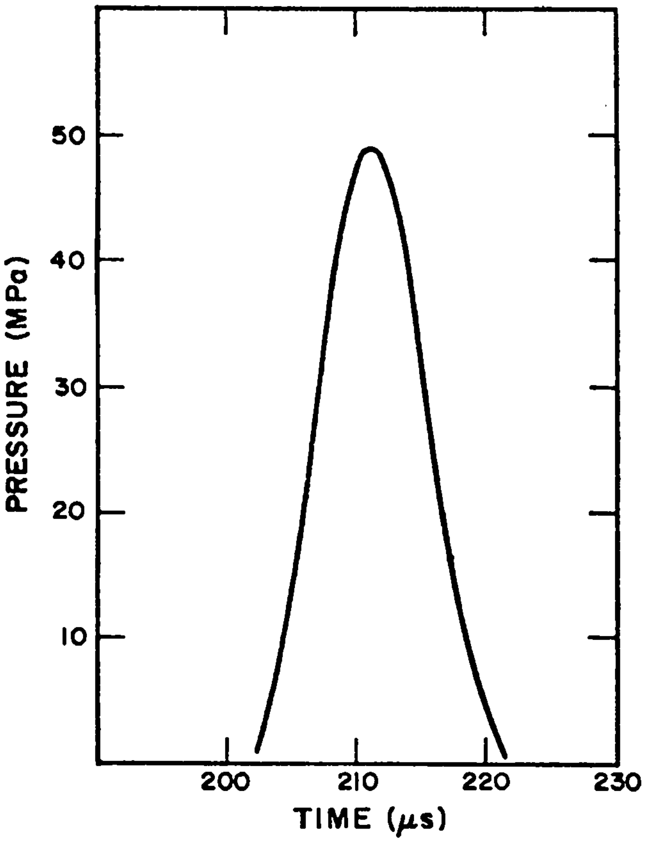

Fig. 18.
Calculated pressure vs equivalent scale time at a test-scale depth of 0.6 m and test-scale range of 0.15 m.

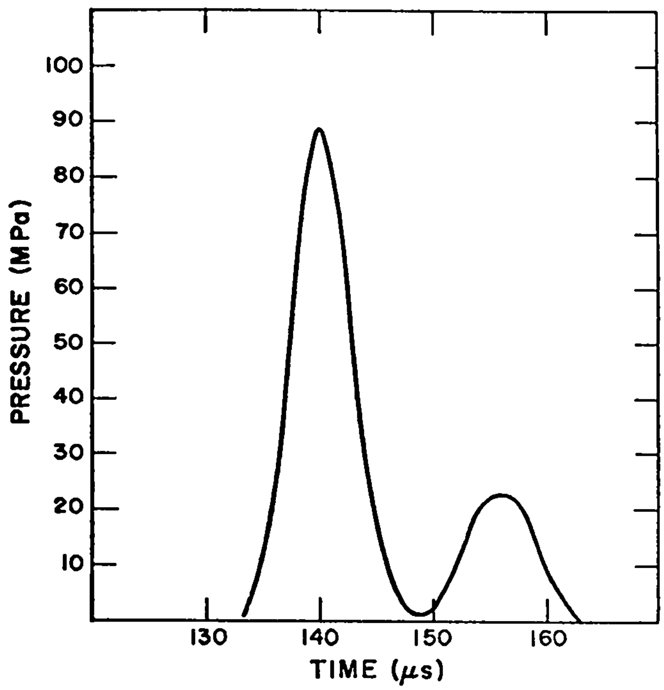

Fig. 20.
Calculated pressure vs equivalent scale time at a test-scale depth of 0.3 m and test-scale range of 0.2 m.

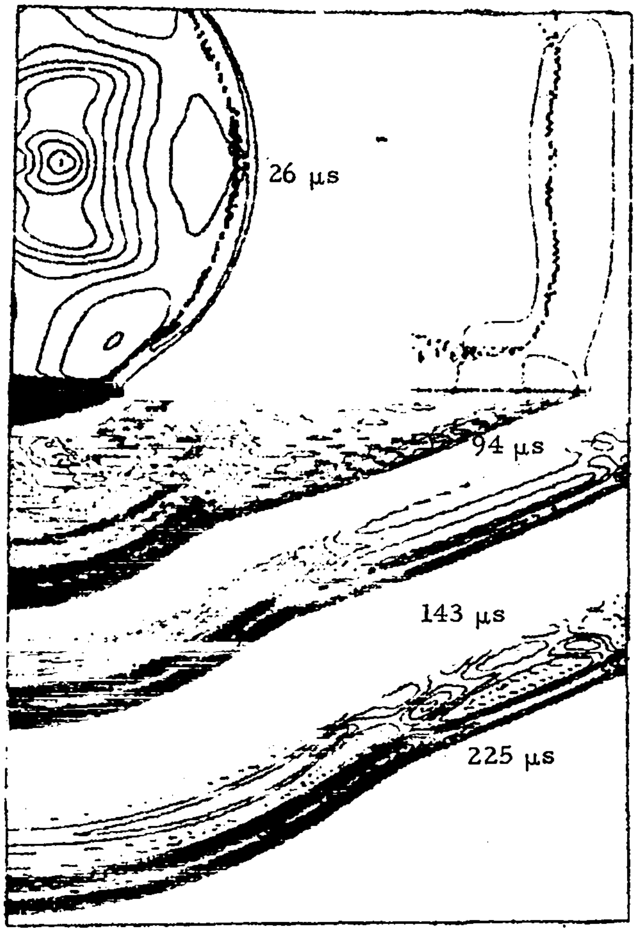

Fig. 21.
Isobar plot.

Peak pressure = 78.4010 MPa at 140.15 μs
Equivalent shock factor = 0.2351
Scale factor = 2.0000
Test-scale shock factor = 0.3325

0.5 m Deep on Axis
Impulse flux = 615.0471 Pa-s
Acoustic impedance = 1.450 (kg/m³)(m/s)
Energy flux = 18688.5289 m-Pa
Effective duration = 20.50 μs
Peak pressure = 60.7120 MPa at 172.90 μs
Equivalent shock factor = 0.1858
Scale factor = 2.0000
Test-scale shock factor = 0.2628

0.6 m Deep on Axis
Impulse flux = 500.7216 Pa-s
Acoustic impedance = 1.450 (kg/m³)(m/s)
Energy flux = 12297.5713 m-Pa
Effective duration = 20.63 μs
Peak pressure = 49.1710 MPa at 206.16 μs
Equivalent shock factor = 0.1513
Scale factor = 2.0000
Test-scale shock factor = 0.2139

0.6 m Deep and 0.15 m From Axis
Impulse flux = 477.1820 Pa-s
Acoustic impedance = 1.450 (kg/m³)(m/s)
Energy flux = 11771.7576 m-Pa
Effective duration = 19.25 μs
Peak pressure = 48.9430 MPa at 211.16 μs
Equivalent shock factor = 0.1477
Scale factor = 2.0000
Test-scale shock factor = 0.2089

0.2 m Deep and 0.2 m From Axis
Impulse flux = 1135.2323 Pa-s
Acoustic impedance = 1.450 (kg/m³)(m/s)
Energy flux = 59677.7598 m-Pa
Effective duration = 27.38 μs
Peak pressure = 132.2500 MPa at 95.65 μs
Equivalent shock factor = 0.3456
Scale factor = 2.0000
Test-scale shock factor = 0.4888

0.3 m Deep and 0.2 m From Axis
Impulse flux = 760.8344 Pa-s
Acoustic impedance = 1.450 (kg/m³)(m/s)
Energy flux = 27007.4108 m-Pa
Effective duration = 29.50 μs
Peak pressure = 88.5530 MPa at 140.03 μs
Equivalent shock factor = 0.2333
Scale factor = 2.0000
Test-scale shock factor = 0.3300

Note that for both the 0.5 and 0.25-cm meshes the Pentolite was burned using the Arrhenius burn technique with an activation energy of 4×10^4 and a frequency factor of 10^{14}. The equation-of-state constants used for Pentolite, air, and water, respectively, are given in Tables II-IV. The nomenclature for these constants is the same as that in Ref. 2.

TABLE II

HOM EQUATION-OF-STATE CONSTANTS FOR PENTOLITE

C	+2.715 000 000 000 E−01	D	−1.914 025 742 150 E−02
S	+2.576 000 000 000 E+00	E	+1.133 678 860 060 E−04
F_s	−8.666 184 955 520 E+00	K	−1.547 367 012 310 E+00
G_s	−5.813 378 220 089 E+01	L	+5.018 764 167 700 E−01
H_s	−6.971 634 108 500 E+01	M	+6.759 910 061 870 E−02
I_s	−8.200 991 027 830 E+00	N	+4.590 841 682 030 E−03
J_s	+2.071 955 690 080 E+01	O	+1.192 771 659 190 E−04
γ_s	+6.747 000 000 000 E−01	Q	+7.637 019 889 560 E+00
C_v	+4.000 000 000 000 E−01	R	−4.405 238 138 730 E−01
V_0	+6.060 606 060 610 E−01	S	+9.469 897 504 470 E−02
α	+0.000 000 000 000 E+00	T	−1.080 604 872 290 E−02
A	−3.488 759 343 020 E+00	U	+3.083 988 173 590 E−04
B	−2.364 864 404 730 E+00	C'_v	+5.000 000 000 000 E−01
C	+2.594 830 803 240 E−01	Z	+1.000 000 000 000 E−01

TABLE III

HOM EQUATION-OF-STATE CONSTANTS FOR AIR

A	−4.510 809 376 830 E+00	O	−2.279 491 657 350 E−06
B	−1.240 596 210 360 E+00	Q	+8.221 295 101 680 E+00
C	+1.371 397 782 080 E−02	R	−2.179 031 685 410 E−01
D	+1.073 345 134 650 E−02	S	−2.231 079 210 530 E−02
E	−1.652 750 544 880 E−03	T	+1.216 411 570 520 E−02
K	−1.630 289 075 940 E+00	U	−1.740 036 607 790 E−03
L	+8.858 093 411 170 E−02	C'_v	+5.000 000 000 000 E−01
M	+2.339 225 632 710 E−03	Z	+1.000 000 000 000 E−01
N	−8.058 850 753 600 E−05	V_0	+7.770 000 000 000 E+02
		P_0	+1.000 000 000 000 E−06

TABLE IV

HOM EQUATION-OF-STATE CONSTANTS FOR WATER

C	+1.483 000 000 000 E−01	J_s	+6.013 303 448 490 E+01
S	+2.000 000 000 000 E+00	γ_s	+1.000 000 000 000 E−01
F_s	+5.720 595 490 370 E+00	C_v	+1.000 000 000 000 E+00
G_s	+6.926 305 732 530 E−01	V_0	+1.000 000 000 000 E+00
H_s	+8.813 944 523 840 E+00	α	+2.000 000 000 000 E−04
I_s	+3.601 198 047 150 E+01		

III. HE, AIR, AND PLEXIGLAS (SLAB GEOMETRY)

A HE, air, and Plexiglas system in slab geometry was studied numerically using the one-dimensional reactive-flow hydrodynamic Lagrangian code called SIN[8] and 2DE.

The physical quantity of interest was the pressure induced in the Plexiglas as a function of time and distance from the PBX 9404 charge. The equation-of-state constants used for air, PBX 9404, and Plexiglas, respectively, are given in Tables III, V, and VI. Figure 22 shows the experimental arrangement. The numerical model is, of course, the same except that two-dimensional effects are neglected.

The SIN hydrodynamic calculations were made in slab geometry for 5.08 cm of PBX 9404 divided into 700 space increments (cells) and 4.00 cm of Plexiglas composed of 200 cells. The air column was divided into 10 cells. Four numerical runs were performed with the air column lengths specified to be 7.62, 15.24, 22.86, and 30.48 cm. The PBX 9404 explosive was burned using a gamma-law Taylor wave technique with a detonation velocity of 0.88 cm/μs. The C-J pressure was 0.3612 Mbar, and γ was 2.9536. The downstream face of the Plexiglas was taken to be a free surface boundary, whereas the HE-P-80 interface was specified to be a piston boundary with a final velocity of zero.

TABLE V

HOM EQUATION-OF-STATE CONSTANTS FOR PBX 9404

C	+2.423 000 000 000 E−01	D	+1.390 835 785 080 E−02
S	+1.833 000 000 000 E+00	E	−1.139 630 240 750 E−02
F_s	−9.041 872 220 420 E+00	K	−1.619 130 411 330 E+00
G_s	−7.131 852 524 350 E+01	L	+5.215 185 341 920 E−01
H_s	−1.252 049 793 600 E+02	M	+6.775 065 941 070 E−02
I_s	−9.204 241 776 030 E+01	N	+4.265 242 646 910 E−03
J_s	−2.218 938 257 270 E+01	O	+1.046 799 999 020 E−04
γ_s	+6.750 000 000 000 E−01	Q	+7.364 229 197 900 E+00
C_v	+4.000 000 000 000 E−01	R	−4.936 582 223 890 E−01
V_0	+5.422 993 492 410 E−01	S	+2.923 530 609 610 E−02
α	+5.000 000 000 000 E−05	T	+3.302 774 022 190 E−02
A	−3.539 062 599 640 E+00	U	−1.145 324 982 060 E−02
B	−2.577 375 903 930 E+00	C'_v	+5.000 000 000 000 E−01
C	+2.600 754 233 320 E−01	Z	+1.000 000 000 000 E−01

TABLE VI

HOM EQUATION-OF-STATE CONSTANTS FOR PLEXIGLAS

C	+2.432 000 000 000 E−01	J_s	−1.467 081 937 390 E+01
S	+1.578 500 000 000 E+00	γ_s	+2.157 000 000 000 E+00
F_s	+5.293 802 435 060 E+00	C_v	+3.500 000 000 000 E−01
G_s	−4.249 503 713 680 E+00	V_0	+8.474 576 270 000 E−01
H_s	−1.550 555 763 320 E+01	α	+1.000 000 000 000 E−04
I_s	−3.086 380 755 720 E+01		

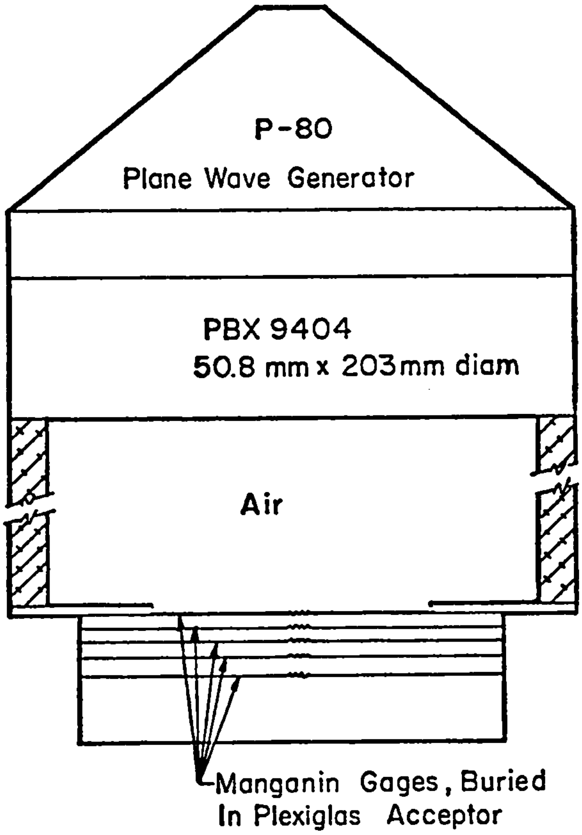

Fig. 22.
Experimental arrangement (not to scale) for the HE, air, and Plexiglas system in slab geometry.

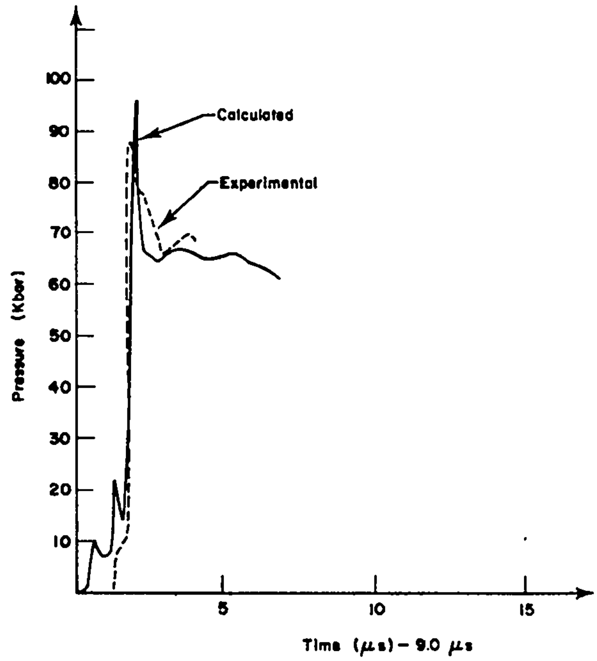

Fig. 23.
Calculated and experimental pressure vs time at a gauge depth of 0.32 cm and 7.62 cm of air. The initial air shock arrival time is 9.0 μs.

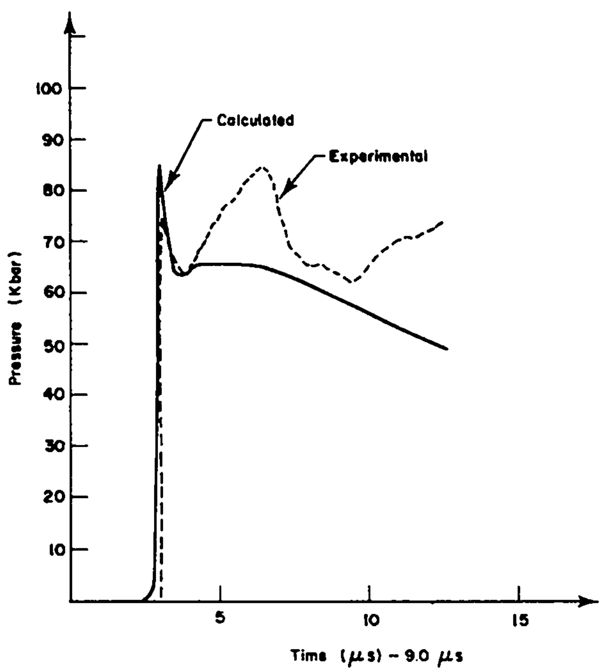

Fig. 24.
Calculated and experimental pressure vs time at a gauge depth of 1.00 cm and 7.62 cm of air. The initial shock arrival time is 9.0 μs.

The Eulerian calculation was performed using a 0.254-cm mesh to simulate the mesh required for two-dimensional simulations of sympathetic and detonation, air, and water shock problems.

The calculated pressure profiles vs time and various gauge depths are shown in Figs. 23-35. Figure 27 is the pressure profile for a 7.62-cm-long air column and a gauge depth of 2.39 cm as calculated by the 2DE code. In all the figures, the abscissa is in microseconds as measured from the impact of the HE-initiated air shock on the first cell of the upstream, or air-Plexiglas, interface.

Certain general features are evident from the data presented in the figures.

(1) Peak calculated pressures, due to the detonation products shock wave (DPSW), are slightly higher than the measured pressures.

(2) Inclusion of rarefactions generated by shock wave impact on the downstream Plexiglas

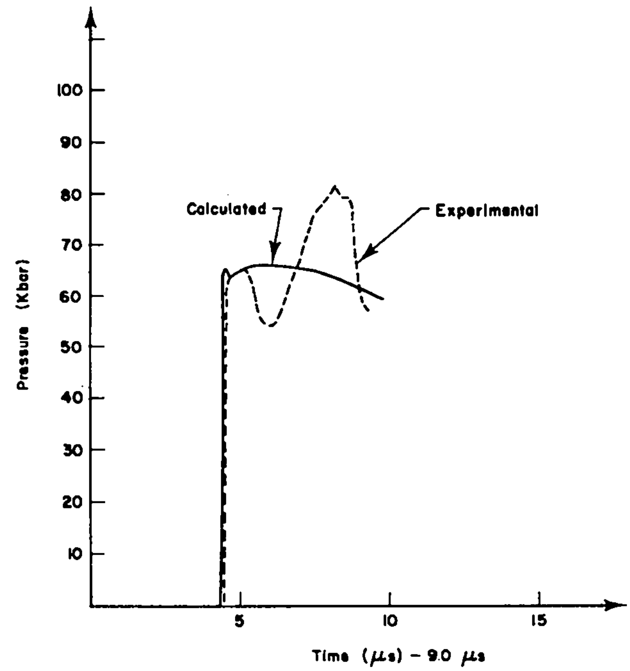

Fig. 25.
Calculated and experimental pressure vs time at a gauge depth of 1.69 cm and 7.62 cm of air. The initial air shock arrival time is 9.0 μs.

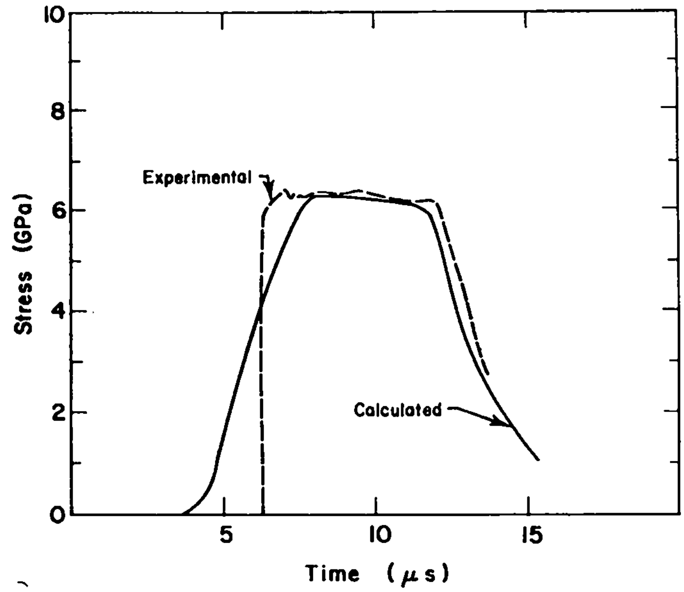

Fig. 27.
Code 2DE calculated pressure and experimental pressure vs time at a gauge depth of 2.39 cm and 7.62 cm of air. The mesh size is 0.254 cm.

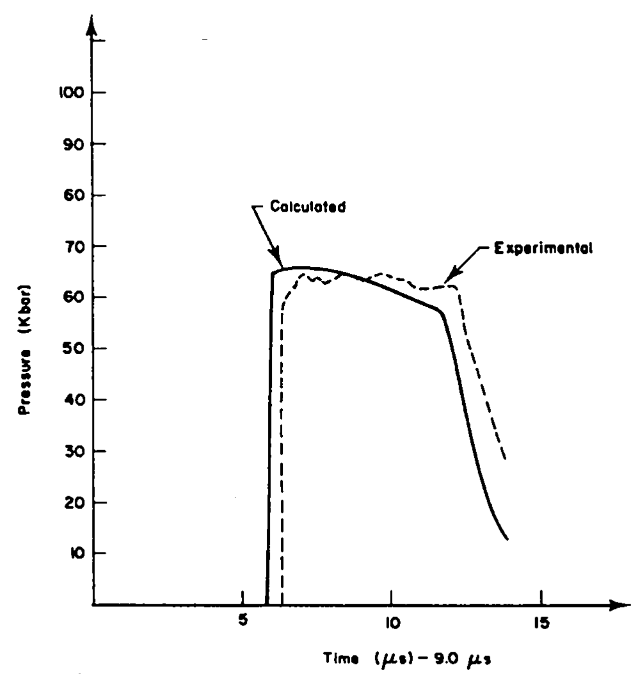

Fig. 26.
Calculated and experimental pressure vs time at a gauge depth of 2.39 cm and 7.62 cm of air. The initial air shock arrival time is 9.0 μs.

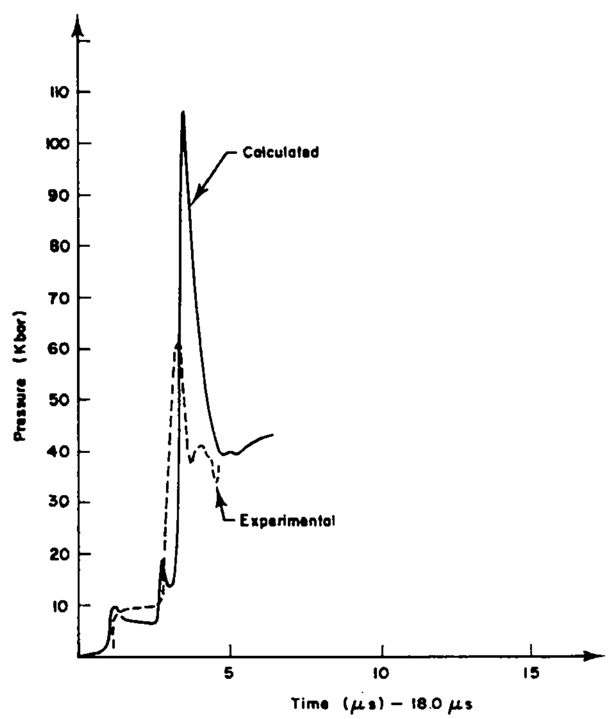

Fig. 28.
Calculated and experimental pressure vs time at a gauge depth of 0.32 cm and 15.24 cm of air. The initial air shock arrival time is 18.0 μs.

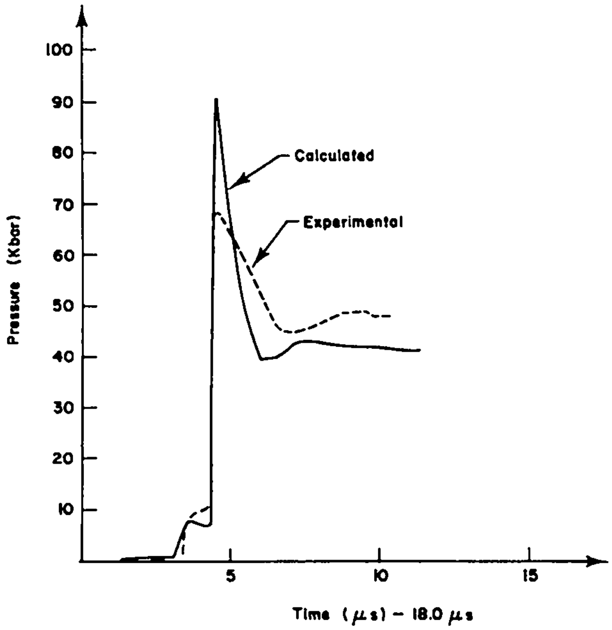

Fig. 29.
Calculated and experimental pressure vs time at a gauge depth of 1.00 cm and 15.24 cm of air. The initial air shock arrival time is 18.0 μs.

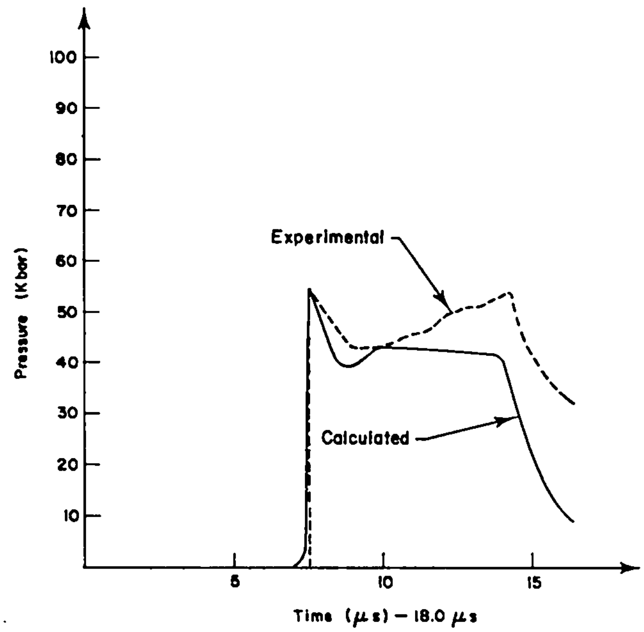

Fig. 31.
Calculated and experimental pressure vs time at a gauge depth of 2.39 cm and 15.24 cm of air. The initial air shock arrival time is 18.0 μs.

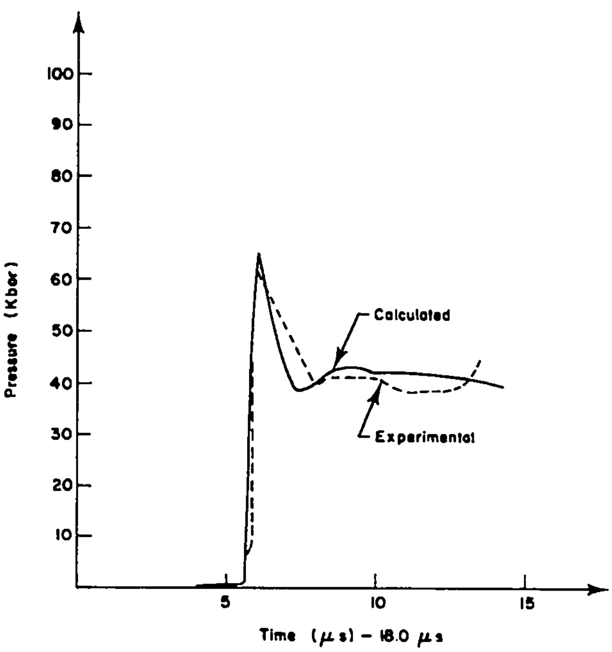

Fig. 30.
Calculated and experimental pressure vs time at a gauge depth of 1.69 cm and 15.24 cm of air. The initial air shock arrival time is 18.0 μs.

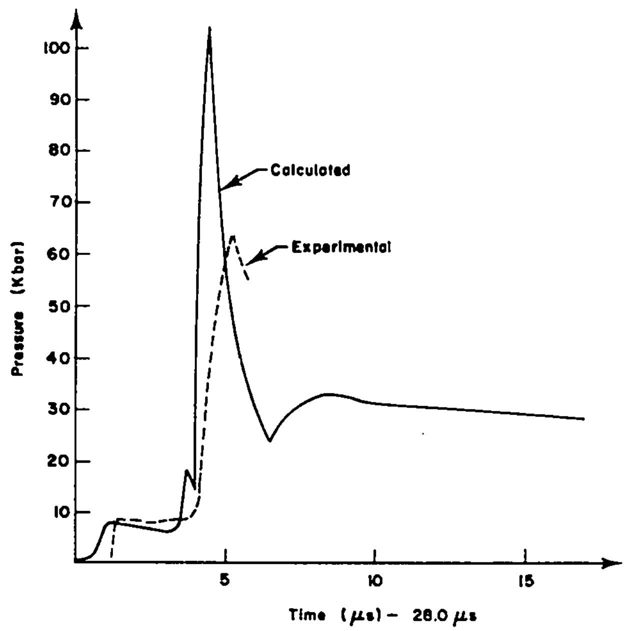

Fig. 32.
Calculated and experimental pressure vs time at a gauge depth of 0.31 cm and 22.86 cm of air. The initial air shock arrival time is 28.0 μs.

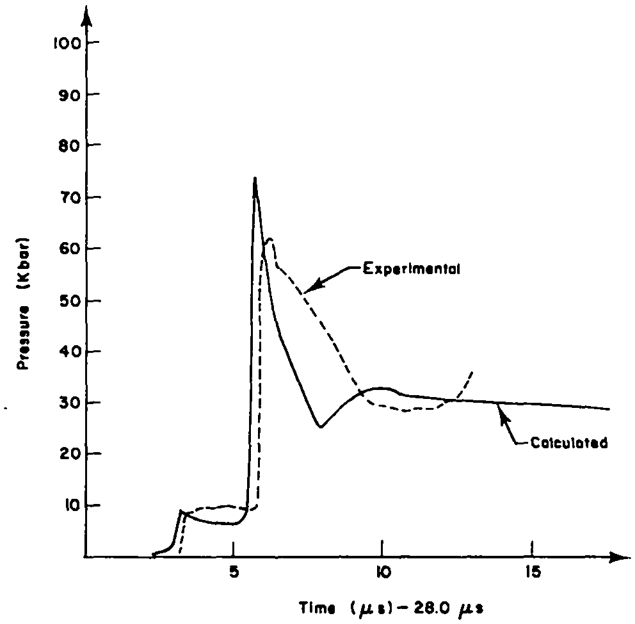

Fig. 33.
Calculated and experimental pressure vs time at a gauge depth of 0.97 cm and 22.86 cm of air. The initial air shock arrival time is 28.0 μs.

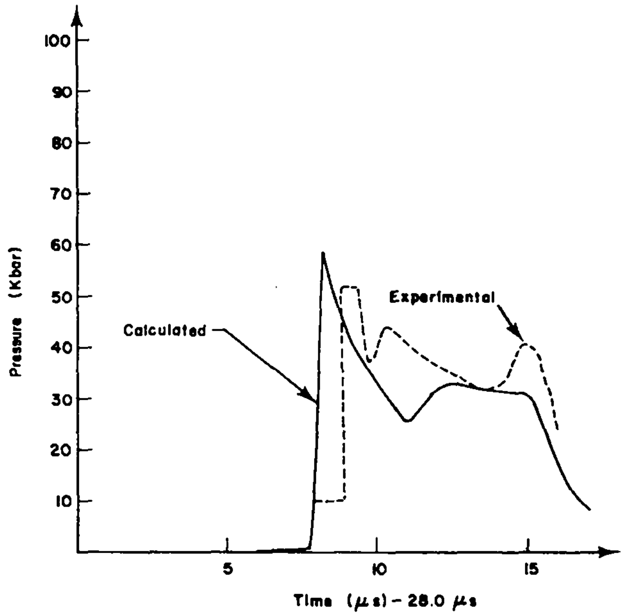

Fig. 35.
Calculated and experimental pressure vs time at a gauge depth of 2.34 cm and 22.86 cm of air. The initial air shock arrival time is 28.0 μs.

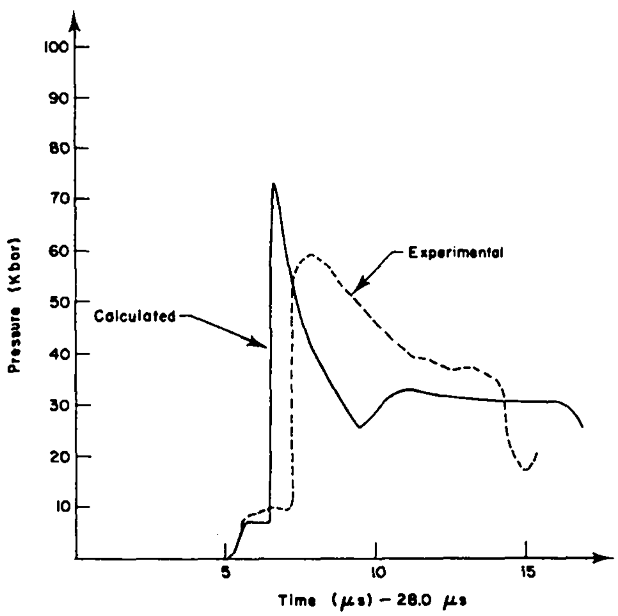

Fig. 34.
Calculated and experimental pressure vs time at a gauge depth of 1.64 cm and 22.86 cm of air. The initial air shock arrival time is 28.0 μs.

face (a free surface boundary) is absolutely essential for predicting long-time pressure decrease.

(3) There are two major shocks—the initial air shock and the final shock resulting from reverberations between the detonation product/air and Plexiglas/air interfaces. The air shock is about 10 kbar, whereas the detonation product shock is roughly an order of magnitude greater. Furthermore, the air shock is driven by the detonation products. Thus with increasing separation between the HE and Plexiglas (but allowing for rarefactions), the air shock wave persists longer.

(4) Experimental data from Figs. 24 and 25 indicate the presence of other peaks after the DPSW peak occurs, but *all* of the calculated data and the rest of the experimental data indicate their absence. Therefore, we conclude that these aftershocks are probably experimental artifacts.

(5) Given large separations between HE and Plexiglas (for example, 22.86 cm), experimental and theoretical arrival times for the

DPSW peaks disagree obviously, although arrival times of the air shock wave peaks still agree well. These two facts taken together indicate that two-dimensional effects become more important (as expected) at large separations.

Thus we find that for the HE, air, and Plexiglas experimental arrangement shown in Fig. 22 (slab geometry) we can calculate the gross features and detailed structure of the shock waves induced in the Plexiglas by the HE detonation.

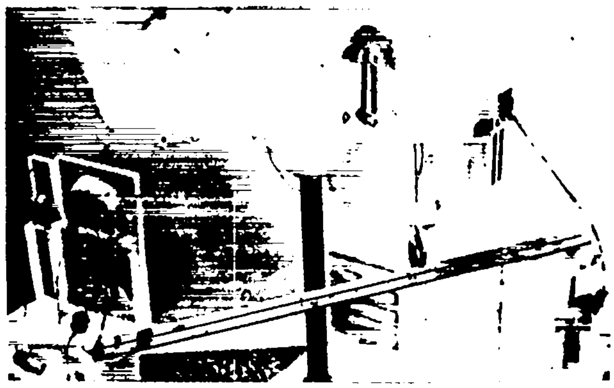

Fig. 36.
Actual experimental arrangement for the HE, air, and Plexiglas system in spherical geometry.

IV. HE, AIR, AND PLEXIGLAS (SPHERICAL GEOMETRY)

A HE, air, and Plexiglas system in spherical geometry (detonating spherical charge) was studied numerically using SIN. As in the slab case, the physical quantity of interest was the pressure induced in the Plexiglas as a function of time and distance from a spherically symmetric PBX 9404 charge. The equation-of-state constants used were the same as those for slab geometry (Tables III, V, and VI).

The actual experimental arrangement is shown in Fig. 36; Fig. 37 is a schematic (not to scale).

The SIN hydrodynamic calculations were made in spherical geometry for a 3.81-cm-radius ball of PBX 9404 divided into 540 space increments (cells), an air gap divided into 10 cells, and 1.91 cm of Plexiglas composed of 200 cells. Numerical runs were performed with the air gap specified to be 3.18, 6.99, 10.80, and 15.24 cm. The PBX 9404 explosive was burned using the CJ volume burn technique with a burn volume of 0.4054 cm^3/g and a detonation velocity of 0.88 cm/μs. The downstream face of the Plexiglas was taken to be a free surface boundary, and the gauge was 0.635-cm deep in the Plexiglas.

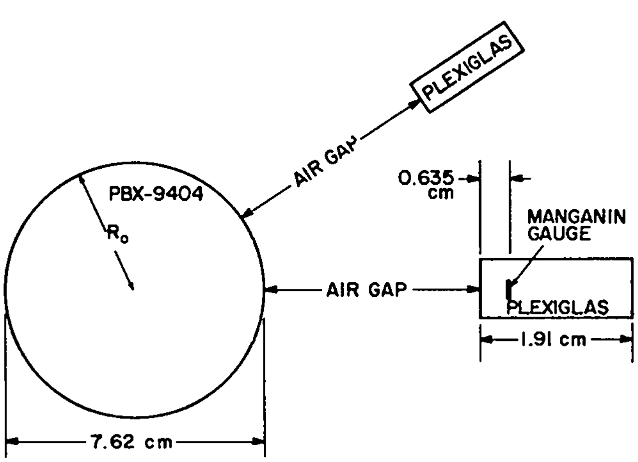

Fig. 37.
Schematic of experimental arrangement (not to scale) for the HE, air, and Plexiglas system in spherical geometry.

Note that (1) for each air gap, we put two gauges in the Plexiglas to try to ensure reproducibility; (2) the experimental time base began with "break-out" at the explosive surface of the detonating sphere, whereas the calculational time base began with initiation of detonation; (3) the experimental pressure profiles were obtained from two separate runs—the 3.18- and 10.80-cm air gap measurements in run No. 1, and the 6.99- and 15.24-cm ones in run No. 2; (4) the pressure profile induced in the Plexiglas (both experimental and calculational) for each air gap results from a combination of the air shock wave, detonation products shock wave, and reverberations.

Figures 38-49 show calculated and experimental pressure profiles as a function of time and various gauge depths. Figure 50 shows peak overpressure vs R/R_0 as derived from the calculated pressure profiles (R_0 = radius of donor charge, R = distance from center of donor charge). Figure 51 shows a

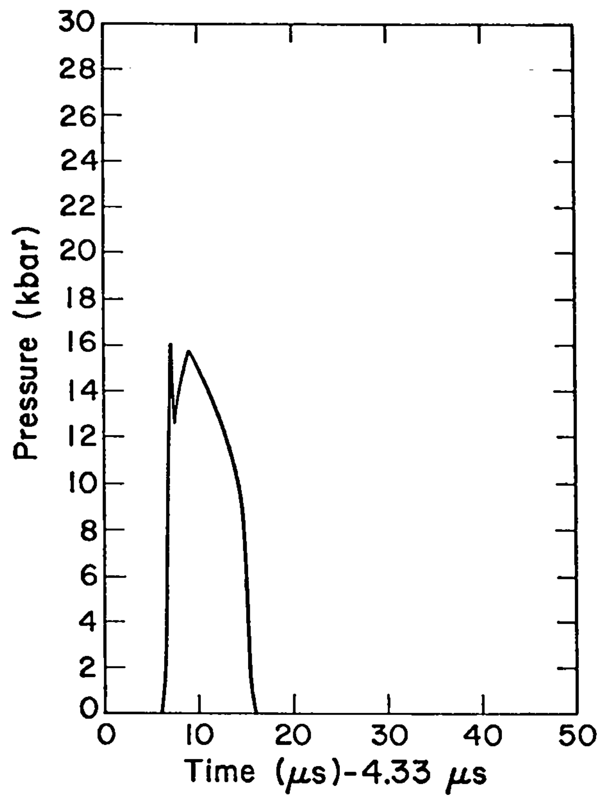

Fig. 38.
Calculated pressure vs time from breakout (3.18-cm air gap).

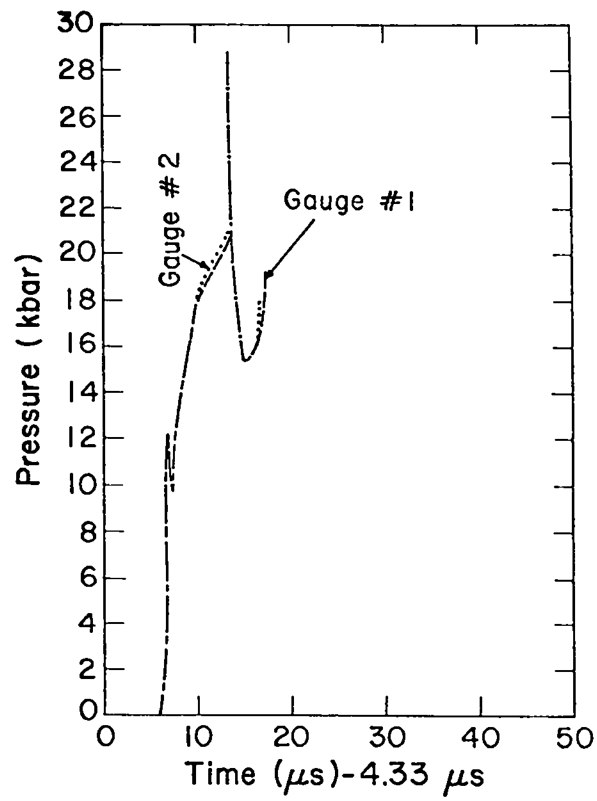

Fig. 39.
Experimental pressure vs time from breakout (3.18-cm air gap).

power law fit to the data of Fig. 50, and Fig. 52 compares the data of Figs. 50 and 51.

The figures show that experimental and calculated pulse width, arrival time, and peak pressure generally agree reasonably well. (These three quantities are, in fact, the most critical for most applications.)

This conclusion is reinforced by the degree of non-reproducibility of the pressure gauge data. Figures 39 and 40, especially, show a large, anomalous spike in the pressure which has no reasonable explanation other than "noise." Indeed, assuming that the spike is due to noise and assigning it a strongly peaked Gaussian shape gives a good overall fit to the calculated pressure profile.

The shock waves induced in the Plexiglas by the initial air shock wave (IASW) show clearly in Figs. 44-49 for the 10.80- and 15.24-cm air gaps and are about 2 and 1.2 kbar, respectively, whereas the shock wave induced in the Plexiglas by the DPSW is roughly three times larger. In Figs. 38-43 however, the IASW is completely dominated by the DPSW.

A two-peak structure is manifest in all the experimental and calculational results except perhaps those for the 15.24-cm air gap in which the second peak appears as a "rounded" shoulder.

From the data presented so far, both calculational and experimental, we can draw several conclusions.

(1) For the sympathetic detonation problem, the IASW, per se, is not a factor in initiating an acceptor charge located a distance R from the center of the donor charge such that $R \gtrsim 3R_0$, where R_0 is the radius of the donor charge. Since for $R \gtrsim 3R_0$, the IASW amplitude is much less than that of the DPSW, we infer that the IASW is important only because of its ability to preshock an acceptor charge and its possible role in the formation of the two-peak structure of the DPSW. Since the DPSW is so large compared with the IASW,

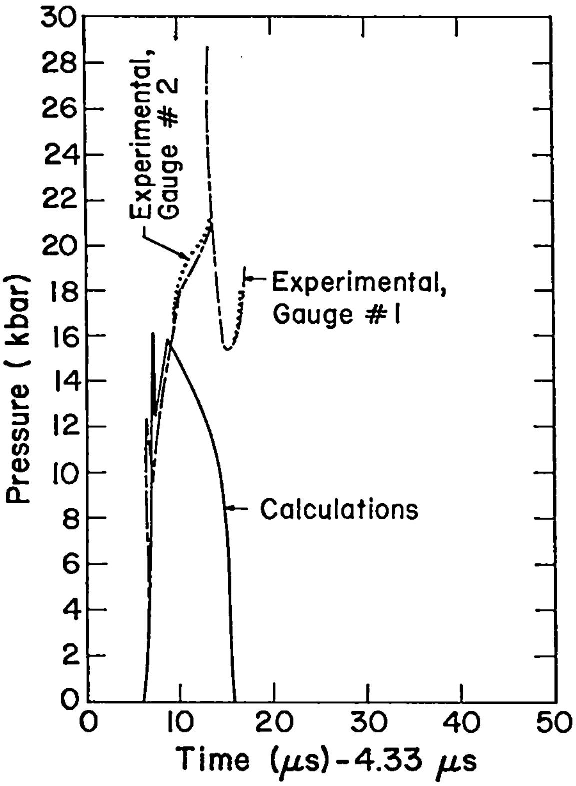

Fig. 40.
Calculated and experimental pressure vs time from breakout (3.18-cm air gap).

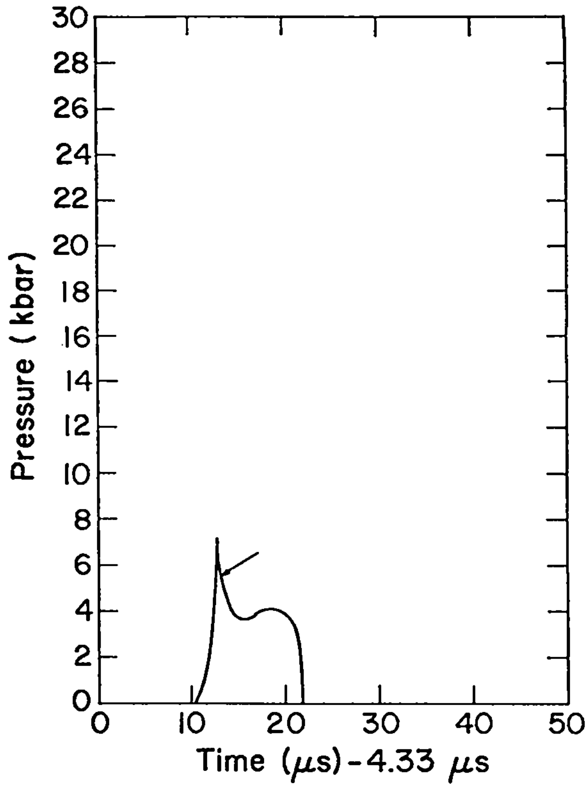

Fig. 41.
Calculated pressure vs time from breakout (6.99-cm air gap).

preshock effects produced in the acceptor charge (Plexiglas) must certainly be considered. Note that no two- or many-peak structure of statistical significance was seen in the analogous slab geometry calculation, implying that the two- or many-peak DPSW structure is related to use of a diverging geometry.

(2) Note that the peak overpressure plotted against R/R_0 can be fitted very well by a power law.

$$P = a(R/R_0)^b \quad ,$$

where

a = 42.76 kbar,

b = −1.506,

P = peak overpressure.

The regression coefficient is 0.98 for this fit to calculated pressures. Thus we find that the gross features and detailed structure of the shock waves induced in the Plexiglas can be calculated successfully in spherical geometry.

V. CONCLUSIONS

We conclude confidently that, with our 2DE and SIN codes and our equations of state, we can calculate pressure vs time profiles and resultant physical quantities of interest accurately and effectively in slab, cylindrical, and spherical geometries and a variety of physical configurations.

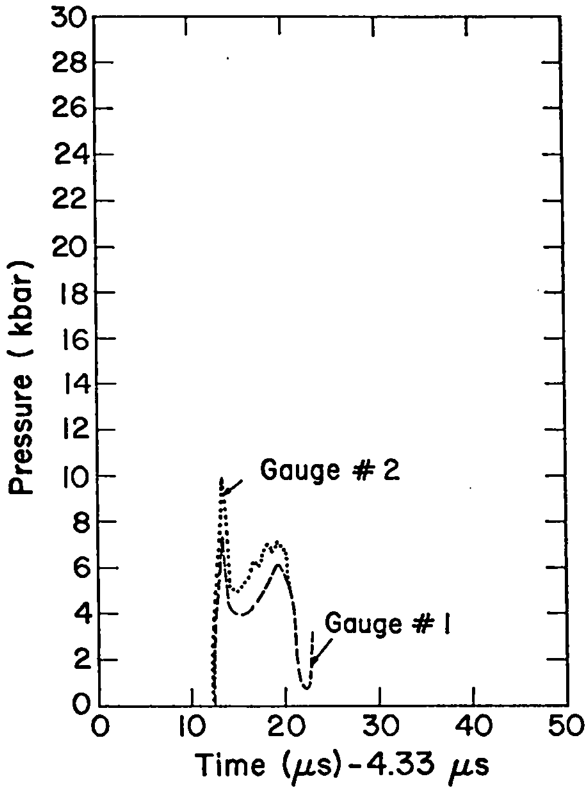

Fig. 42.
Experimental pressure vs time from breakout (6.99-cm air gap).

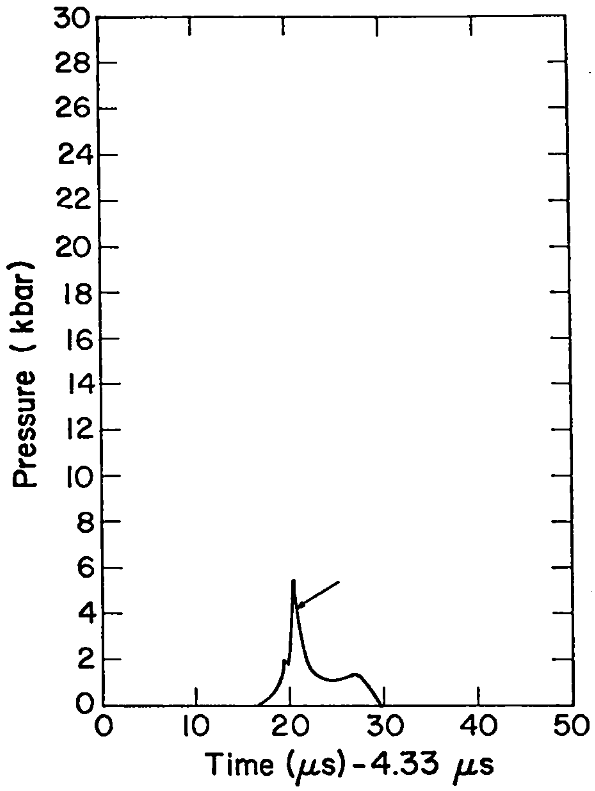

Fig. 44.
Calculated pressure vs time from breakout (10.80-cm air gap).

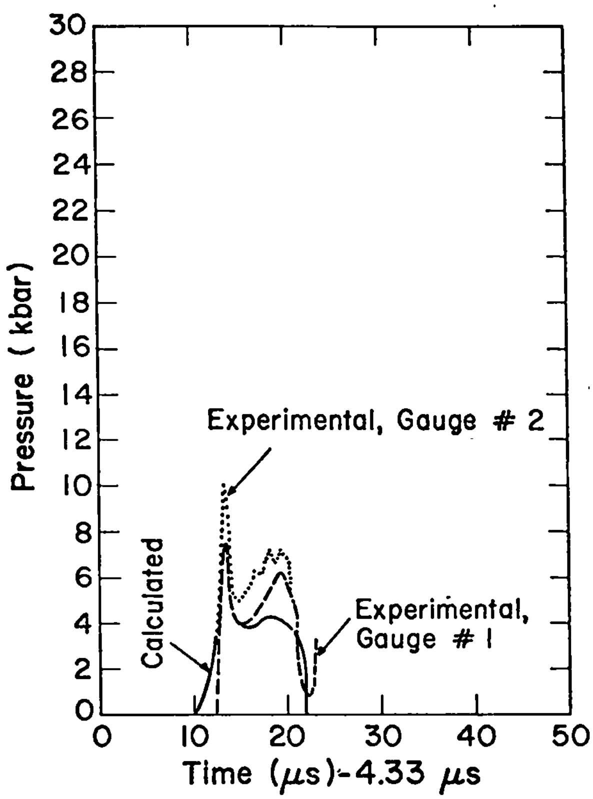

Fig. 43.
Calculated and experimental pressure vs time from breakout (6.99-cm air gap).

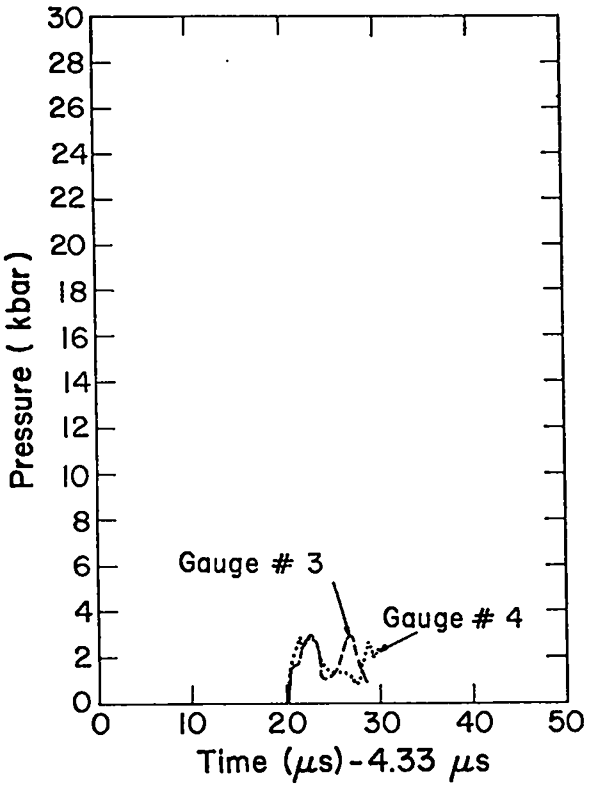

Fig. 45.
Experimental pressure vs time from breakout (10.80-cm air gap).

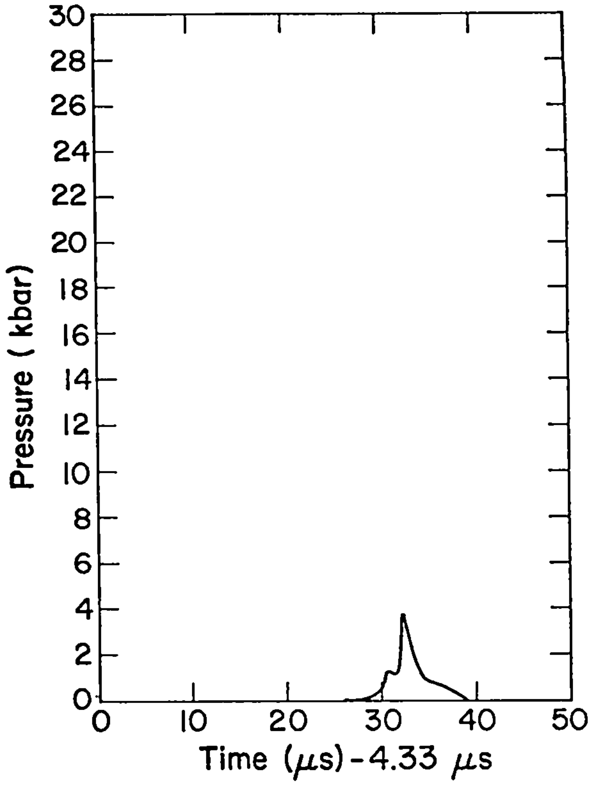

Fig. 47.
Calculated pressure vs time from breakout (15.24-cm air gap).

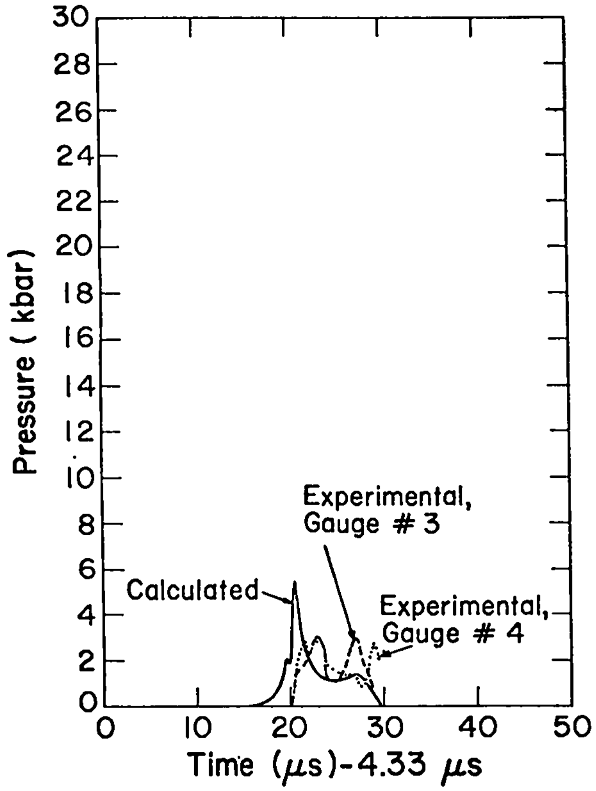

Fig. 46.
Calculated and experimental pressure vs time from breakout (10.80-cm air gap).

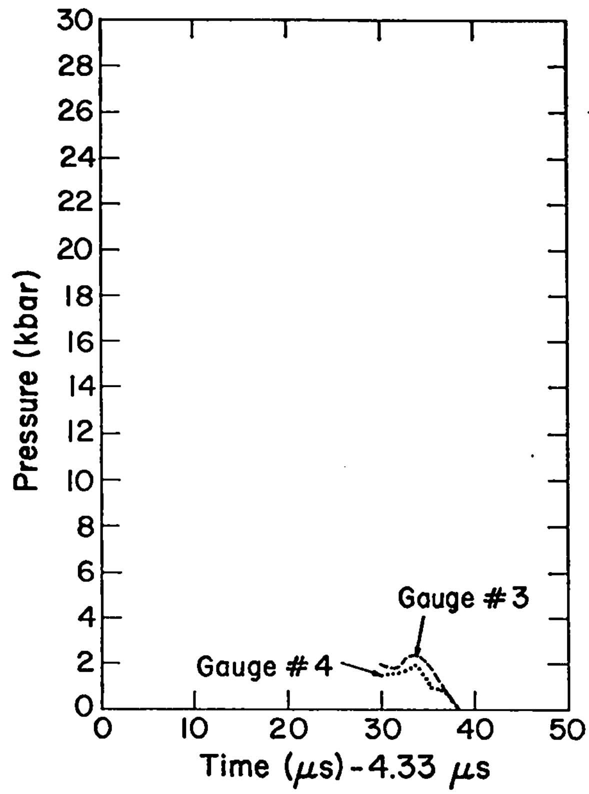

Fig. 48.
Experimental pressure vs time from breakout (15.25-cm air gap).

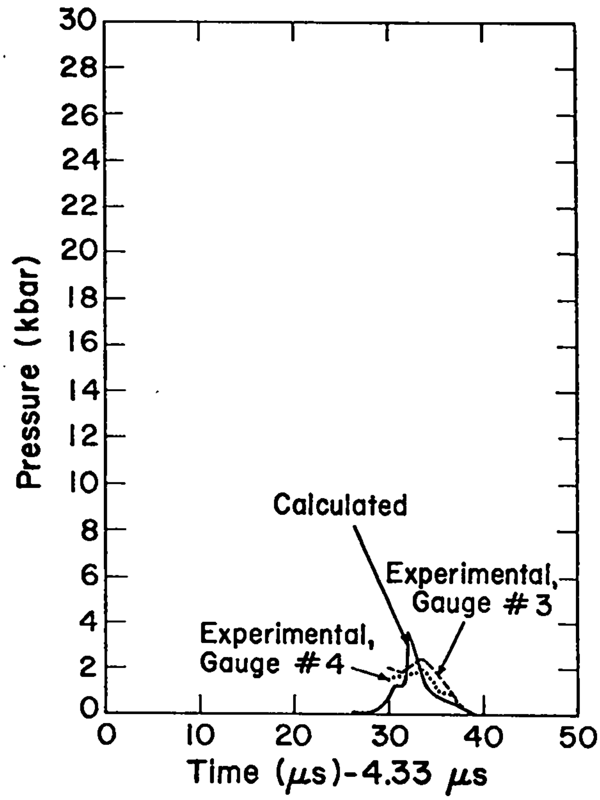

Fig. 49.
Calculated and experimental pressure vs time from breakout (15.24-cm air gap).

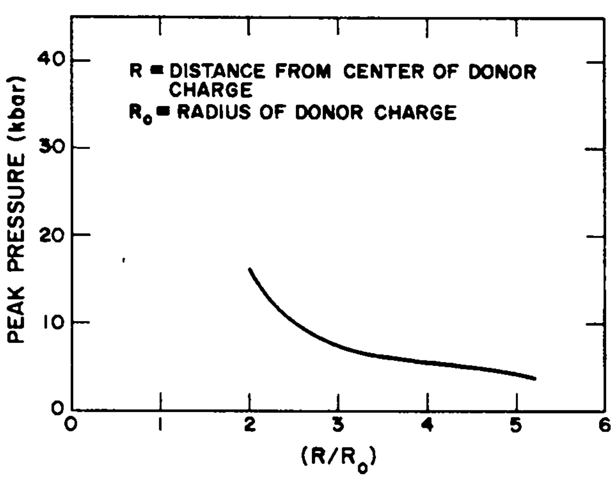

Fig. 50.
Calculated peak pressure vs R/R_0.

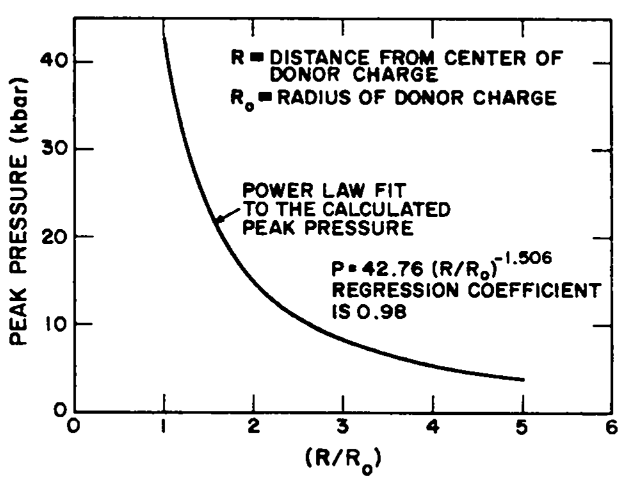

Fig. 51.
Fit to the calculated peak pressure vs R/R_0.

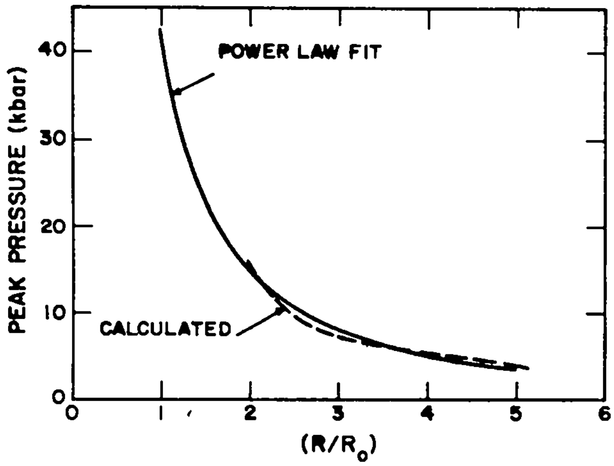

Fig. 52.
Fit and calculated peak pressure vs R/R_0.

REFERENCES

1. Joseph F. Pittman, Naval Surface Weapons Center, unpublished data.

2. J. D. Kershner and C. L. Mader, "2DE, A Two-Dimensional Continuous Eulerian Hydrodynamic Code for Computing Multicomponent Reactive Hydrodynamic Problems," Los Alamos Scientific Laboratory report LA-4846 (1972).

3. Charles L. Mader and William R. Gage, "FORTRAN SIN, A One-Dimensional Hydrodynamic Code for Problems Which Include Chemical Reactions, Elastic-Plastic Flow, Spalling, and Phase Transitions," Los Alamos Scientific Laboratory report LA-3720 (1967).

Printed in the United States of America. Available from
National Technical Information Service
US Department of Commerce
5285 Port Royal Road
Springfield, VA 22161

Microfiche $3.00

001-025	4.00	126-150	7.25	251-275	10.75	376-400	13.00	501-525	15.25
026-050	4.50	151-175	8.00	276-300	11.00	401-425	13.25	526-550	15.50
051-075	5.25	176-200	9.00	301-325	11.75	426-450	14.00	551-575	16.25
076-100	6.00	201-225	9.25	326-350	12.00	451-475	14.50	576-600	16.50
101-125	6.50	226-250	9.50	351-375	12.50	476-500	15.00	601-up	

Note: Add $2.50 for each additional 100-page increment from 601 pages up.